

Hydrodynamic Simulations of the Bardeen–Petterson Effect

Richard P. Nelson [★] & John C.B. Papaloizou [†]

Astronomy Unit, Queen Mary & Westfield College, Mile End Rd, London E1 4NS

Received *****, in original form *****

ABSTRACT

We present SPH simulations of accretion discs in orbit about rotating compact objects, such as black holes and neutron stars, and study the structure of warped discs produced by the Bardeen-Petterson effect. We calculate the transition radius out to which the disc specific angular momentum vector is aligned with that of the black hole. We focus on the parameter regime where the warp dynamics are controlled by bending wave propagation, but also consider models in which warps are subject to diffusion rather than wave transport, and are able to consider the fully nonlinear regime.

Because of hydrodynamic or pressure effects, for the parameter range investigated, the transition radius is always found to be much smaller than that obtained by Bardeen & Petterson (1975). For discs with midplane Mach numbers of ~ 10 , the transition occurs between $10 - 16 R_+$ (gravitational radii), whereas for a Mach number of ~ 30 it occurs at around $30 R_+$. A thicker disc with a Mach number of 5 is found to produce no discernible warped structure.

The rate of black hole – disc alignment is found to be consistent with the ideas of Rees (1978), with the alignment torque behaving as if it arises from the accreted material transferring its misaligned component of angular momentum at the larger transition radius of Bardeen & Petterson (1975).

The inclusion of Einstein precession in the calculations modified both the warped disc structure and, consistent with linear analysis, produced an increased alignment rate by up to a factor of 4 because of the effect that the non Keplerian potential has on the propagation of warps.

Key words: accretion discs-black hole-Bardeen Petterson effect- bending waves-warps- SPH-simulations

1 INTRODUCTION

Accretion discs may occur around stellar mass black holes in X–ray sources such as Cygnus X–1, or around very massive black holes in active galaxies. The Lense-Thirring effect, or dragging of inertial frames, has an important influence on the structure of an accretion disc around a rotating black hole in the situation where the equatorial plane of the outer disc far from the black hole is misaligned with the symmetry plane of the black hole.

Bardeen & Petterson (1975) showed that a viscous disc would be expected to relax to a form in which the inner regions become aligned with the equatorial plane of the black hole out to a transition radius, beyond which the disc remains aligned with the outer disc. This phenomenon may be

important for understanding absorption and reprocessing of X–rays in X–ray sources, and also for providing stability for jet directions in radio sources (Rees 1978).

In their calculation Bardeen & Petterson (1975) assumed that the warps in the misaligned disc diffused on a viscous time scale. The viscosity coefficient was taken to be of the the same magnitude as that producing the mass inflow, typically modelled using the standard Shakura & Sunyaev (1973) α prescription. However, Papaloizou and Pringle (1983) showed that for an isotropic viscosity, warp diffusion occurs at a rate faster by $\sim 1/(2\alpha^2)$, provided $\alpha > H/r$, much reducing the transition radius. For $\alpha < H/r$ it is expected that the dynamics is controlled by the wave modes present in the disc.

The location of the transition radius has been investigated in the diffusive linear regime ($\alpha > H/r$) (Kumar & Pringle 1985), and in a model including viscous effects but neglecting pressure (Scheuer & Feiler 1996). The Bardeen–Petterson effect has also been studied in the linear regime,

[★] Email address: R.P.Nelson@qmw.ac.uk

[†] Email address: J.C.B.Papaloizou@qmw.ac.uk

but with $\alpha < H/r$, by Ivanov & Illarianov (1997), where they also considered the effects of some additional post Newtonian corrections.

In this paper we study the Bardeen-Petterson effect using SPH simulations. We focus primarily on the parameter regime where the warp dynamics are controlled by bending wave propagation, although we also examine models in which warps are subject to diffusion and are not transmitted by waves. The properties of the wave and diffusive communication that occurs in the discs modelled here are discussed in detail in a recent paper (Nelson & Papaloizou 1999) hereafter referred to as paper I. In that paper we compare SPH simulations of small amplitude disturbances to results obtained using the linearized fluid equations that are solved using a standard finite difference code, though we comment more generally that by using SPH calculations we are able to consider the fully non linear regime. The calculations presented in paper I are used to calibrate the code viscosity. The warping of a gaseous disc generates vertical shearing motions (*i.e.* horizontal motions that are a function of the vertical position in the disc). The viscosity that acts on this vertical shear may not be the same as that which acts on the usual horizontal shear associated with a planar, differentially rotating accretion disc. We therefore denote the dimensionless viscosity parameter acting on the vertical shear as α_1 , and that acting on the horizontal shear through the r - ϕ component of the stress tensor as α . The test calculations presented in paper I indicate that the thicker discs that we consider, with midplane Mach numbers of $\mathcal{M} \sim 12$, (where $H/r \sim \mathcal{M}^{-1}$) have $\alpha_1 \simeq 0.04$ so that bending waves are expected to propagate in these discs. We note that calibration runs indicate that $\alpha \simeq 0.02 - 0.03$ for disc models of this thickness obtained using SPH (e.g. Larwood *et al.* 1996; Bryden *et al.* 1999). It is found that the thinner discs with $\mathcal{M} \sim 30$ have values of $\alpha_1 \sim 0.1$ and similar values for α so that in these cases warping disturbances are expected to evolve diffusively.

We study the Bardeen-Petterson effect for a variety of disc Mach numbers, and find that the transition radius is always much smaller than that obtained by Bardeen & Petterson (1975). The rate of black hole - disc alignment is, however, found to be consistent with the ideas of Rees (1978), and the later work of Scheuer & Feiler (1996) when taking the viscous diffusion coefficients acting in and out of the plane to be equal. A discussion of this result is presented in section 8.5.

The plan of the paper is as follows. In section 2 we give the basic equations. In section 3 we describe how Lense-Thirring precession acting on a misaligned accretion disc in the neighbourhood of a rotating black hole leads to the Bardeen-Petterson effect, where the inner regions of the disc become aligned with the equatorial plane of the black hole out to the transition radius.

The relaxation of an accretion disc for which the angular momentum vector is misaligned with the spin vector of a rotating black hole is dependent on the dynamics of warps or bending waves (see paper I and references therein). Linear bending waves are expected to propagate if the Shakura & Sunyaev (1973) α viscosity appropriate to dissipation of vertical shear, $\alpha_1 < H/r$. For larger values of α_1 , the evolution is diffusive. In section 4 we consider the relaxation of a

disc subject to gravomagnetic forces when there is a small misalignment.

In section 5 we discuss estimates of the Bardeen-Petterson transition radius based on equating the Lense-Thirring precessional shear rate to the viscous diffusion rate. Here we note that it is the diffusion rate of warps that is important and this occurs at a rate faster by $\sim 1/(2\alpha^2)$ than the standard viscous rate (Papaloizou & Pringle 1983) if an isotropic standard Shakura & Sunyaev (1973) α viscosity is used so $\alpha = \alpha_1$. The transition radius then decreases as α decreases until $\alpha = H/r$. Then the warp diffusion rate becomes the same as the propagation rate of bending waves and the transition radius cannot decrease further as α is reduced.

In section 6 we describe the implementation of SPH used to perform the simulations, and in section 7 we describe the calculations of the Bardeen-Petterson effect. In section 8 we present the results of nonlinear simulations of a disc orbiting around a rotating black hole with Kerr parameter $a = 1$ and which has its spin vector initially misaligned with that of the disc. We use the lowest order post Newtonian approximation in our simulations.

We present simulations for Mach numbers ranging between 5 and 30 and inclinations of the outer disc plane of 10 and 30 degrees. For the effective viscosity α_1 in the disc, in the lower Mach number cases, warps are governed by bending waves, while for the higher Mach number case of 30 they are diffusive.

The central portion of the disc becomes aligned with the equatorial plane of the hole out to a transition radius which was found to be much smaller than that given by Bardeen & Petterson (1975), ranging between 15 and 30 gravitational radii.

Models were considered both at high and low inclination. In the nonlinear high inclination case the transition between the aligned and non-aligned disc was more abrupt than in the low inclination case, indicative of a tendency for the outer part of the disc to become disconnected from the inner part.

A calculation is presented for a disc of substantially larger outer radius than the other disc models we consider. We do not expect that the location of the transition radius will be affected by the location of the outer disc radius provided that it is sufficiently far away from the transition zone. In the majority of cases that we consider, the outer disc radius ($r \sim 2$) is a factor of between three and four times larger than the final transition radius ($r \sim 0.7$). We find that a disc that is more than a factor of three larger again (*i.e.* $r \sim 7$) has a transition radius that is unchanged, indicating that the smaller disc models are sufficiently large to not affect the location of the transition radius.

We go on to investigate the time scale required for black-hole disc alignment. Our results are consistent with the ideas of Rees (1978), and the later work of Scheuer & Feiler (1996) when the viscous diffusion coefficients acting in and out of the plane are taken to be equal, even though the transition radius is much smaller in our case. We also find that the effects of Einstein precession are to increase the alignment rate, as expected from a linear analysis.

Finally in section 9 we summarize our results and conclusions.

2 EQUATIONS OF MOTION

In order to describe a compressible fluid, we adopt continuity and momentum equations in the form

$$\frac{d\rho}{dt} + \rho \nabla \cdot \mathbf{v} = 0 \quad (1)$$

and

$$\frac{d\mathbf{v}}{dt} = -\frac{1}{\rho} \nabla P + \mathbf{v} \times \mathbf{h} - \nabla \Phi + \mathbf{S}_{visc} \quad (2)$$

where

$$\frac{d}{dt} = \frac{\partial}{\partial t} + \mathbf{v} \cdot \nabla \quad (3)$$

denotes the convective derivative, ρ is the density, \mathbf{v} is the velocity, P is the pressure, Φ is the gravitational potential and \mathbf{S}_{visc} represents the viscous force per unit mass. The above equations are the standard Newtonian equations of fluid dynamics apart from the addition of the $\mathbf{v} \times \mathbf{h}$ term to equation (2) which gives the gravomagnetic force per unit mass experienced by the fluid in the vicinity of a rotating black hole to lowest post Newtonian order (e.g. Blandford 1996). Here \mathbf{h} is defined by the expression

$$\mathbf{h} = \frac{2\mathbf{S}}{R^3} - \frac{6(\mathbf{S} \cdot \mathbf{r})\mathbf{r}}{R^5} \quad (4)$$

and

$$\mathbf{S} = \frac{G\mathbf{J}}{c^2}. \quad (5)$$

Here R is the distance to the central mass and \mathbf{r} denotes the coordinate vector measured from there. It is the gravomagnetic force that gives rise to Lense–Thirring precession which in turn leads to the alignment of the rotation axis of a viscous disc with that of the black hole. The spin angular momentum of a Kerr black hole is given by the equation

$$\mathbf{J} = \frac{aGM^2}{c} \hat{\mathbf{k}}, \quad (6)$$

where $\hat{\mathbf{k}}$ denotes the unit vector in the z direction associated with cylindrical coordinates (r, ϕ, z) based on the central mass. Thus $R = \sqrt{(r^2 + z^2)}$. For a maximally rotating hole, the Kerr parameter $a = 1$, with M being the mass of the black hole, and c the speed of light.

Because the effects of interest simulated here take place many gravitational radii from the black hole, relativistic effects are included only in a post Newtonian approximation.

In the calculations described in subsequent sections, different prescriptions for the gravitational force were used. In some cases, a softened Keplerian potential was used such that the gravitational force per unit mass is

$$-\nabla \Phi = -\frac{GM}{(R^2 + b^2)^{3/2}} \mathbf{r} \quad (7)$$

where b is the gravitational softening parameter. This was adopted in order to prevent numerical divergences as the disc material approaches the central object. In other cases, the effects of Einstein precession were included, and the central object was treated as a uniform density sphere of finite size to prevent the gravitational force from becoming infinite as $r \rightarrow 0$. In this case the gravitational force per unit mass outside the sphere was taken to be

$$-\nabla \Phi = -\frac{GM}{R^3} \left(1 + \frac{6R_+}{R}\right) \mathbf{r} \quad (8)$$

where $R_+ = GM/c^2$, denotes the gravitational radius. This force differs from the pseudo-Newtonian expression, often adopted in calculations of this kind, that gives the correct radius of the last stable circular orbit (e.g. Paczynski & Wiita 1980), but instead it gives the correct orbital apsidal precession frequency at large distances from the black hole.

The calculations that included softening of the gravitational force were performed before we arrived at the idea of treating the central object as a uniform density sphere as a means of preventing numerical divergences. Although there is no astrophysical phenomenon that has a direct analogy with the use of a softening parameter as described in equation (7), it plays a relatively small role in our calculations of the Bardeen–Petterson transition zone. The fact that there is an associated retrograde precession changes the behaviour slightly, and this acts as a convenient way of illustrating the effect of the disc rotation profile on the behaviour of warps in accretion discs by comparing the results obtained with softening with those obtained when Einstein precession is included.

These equations are supplemented by an equation of state, which in this case is taken to be a polytrope of index $\gamma = 5/3$:

$$P = K\rho^\gamma. \quad (9)$$

The sound speed is $c_s = \sqrt{dP/d\rho}$. Energy dissipated through the action of artificial viscosity is simply allowed to leave the system, so that a barotropic equation of state is assumed throughout.

3 PRECESSION FREQUENCIES AND THE BARDEEN–PETTERSON EFFECT

The effect of Lense–Thirring precession is to cause the plane of an orbit inclined to the (x, y) plane to precess about the angular momentum (z) axis. If a viscous disc with negligible inertia is set up with its midplane initially misaligned with the (x, y) plane, differential Lense–Thirring precession will lead to the formation of a warped disc. The (prograde) nodal precession frequency that arises due to the inclusion of the gravomagnetic force term in the equation of motion (2) is given by

$$\omega_z = \frac{2S}{R^3}, \quad (10)$$

where $S = |\mathbf{S}|$. Note that this decreases with radius resulting in differential precession.

The Bardeen–Petterson effect is caused by the combined effects of Lense–Thirring precession and internal disc viscosity, which, assuming the disc has negligible inertia, acts to align the midplane of the inner region of the accretion disc with the (x, y) plane. This is because the damping produced by viscosity, acting on the small scale structure (twisting up) produced by strong differential precession, causes the inner disc to settle into the plane of the black hole equator.

However, the outer parts of the disc remain in their original plane because the Lense–Thirring precession rate drops off sharply as r increases, such that the internal pressure and viscous stresses acting in the disc are able to limit the effects of differential precession.

The radius of transition between the two disc midplanes is expected to occur approximately where the rate at which

the disc is twisted up by differential precession is balanced by the rate at which disc warps are diffused or propagated away. The rate at which the disc is twisted up is given by $1/\tau_{dp} = |R(d\omega_z/dR)|$, where τ_{dp} is the differential precession time scale. The rate at which warps are propagated or diffused is discussed in the next section.

Important dynamical effects can also occur because precession of orbital apsidal lines occurs when the central potential is non Keplerian. The two cases considered here are associated with the softening of the central potential and taking into account Einstein precession.

The rate of (retrograde) apsidal precession of a near circular orbit in the softened gravitational potential (7) is given by

$$\omega_{ps} = -\frac{3}{2}\Omega\frac{b^2}{R^2}, \quad (11)$$

where Ω is the circular orbit rotation frequency. It can be seen that the importance of this apsidal precession drops off quickly as $R \gg b$.

The rate of (prograde) Einstein apsidal precession associated with the potential (8) is given by

$$\omega_{pE} = 3\Omega\frac{R_+}{R}. \quad (12)$$

Comparison of these two rates of precession shows that the effects of Einstein precession remain relatively more important further away from the black hole than the effects of gravitational softening.

Our numerical experiments show that use of (8) rather than just a softened potential has a noticeable effect on the results, in particular on the way in which the disc undergoes the transition between the plane occupied by the inner disc and that occupied by the outer disc. This is related to the effects of a non Keplerian potential on the propagation and diffusion of warps.

4 MISALIGNMENT AND THE BARDEEN–PETTERSON TRANSITION

4.1 Small Misalignments at Large Radii

The radius at which the disc midplane undergoes a transition between alignment with the (x, y) plane and its initial inclination at large distance can be simply estimated in the situation when the latter inclination is small. To do this we consider small amplitude bending disturbances of the disc out of the (x, y) plane. These are required to have an inclination that is asymptotically constant and equal to its value at large radii. The theory and propagation of small amplitude bending waves has been discussed in paper I and we may apply the analysis presented there. To make this application we first work on the $\mathbf{v} \times \mathbf{h}$ term in equation (2). Using (4) this may be written

$$\mathbf{v} \times \mathbf{h} = \frac{2S(\mathbf{v} \times \hat{\mathbf{k}})}{R^3} + \frac{6Sz(\mathbf{r} \times \mathbf{v})}{R^5}. \quad (13)$$

For linear disturbances at large radii, we may regard S as a first order quantity and accordingly replace the velocity by the unperturbed Keplerian value in (13). Thus in cylindrical coordinates $\mathbf{v} = (0, v_\phi, 0)$ with $v_\phi = \sqrt{GM/r}$. Additionally as we are interested in a thin disc [neglecting corrections of

order $(H/r)^2$] we replace R by the cylindrical radius r . Then (13) becomes

$$\mathbf{v} \times \mathbf{h} = \frac{2S\sqrt{GM}\hat{\mathbf{r}}}{r^{7/2}} + \frac{6Sz\sqrt{GM}\hat{\mathbf{k}}}{r^{9/2}}. \quad (14)$$

This can be considered [again neglecting corrections of order $(H/r)^2$] to arise from an effective potential such that

$$\mathbf{v} \times \mathbf{h} = -\nabla\Phi_{gr}, \quad (15)$$

with

$$\Phi_{gr} = \frac{4S\sqrt{GM}}{5r^{5/2}} - \frac{3Sz^2\sqrt{GM}}{r^{9/2}}. \quad (16)$$

If we now add this potential to the already existing one we obtain the total potential governing the motion of the fluid

$$\Phi_{Tot} \rightarrow \Phi + \Phi_{gr}. \quad (17)$$

The governing equations are now of the same general form as those describing bending disturbances considered in paper I. We shall consider the low frequency limit incorporating viscosity as in that paper. Accordingly we adopt equation (19) of that paper. This applies to disturbances for which the ϕ and t dependence is through a factor $e^{i(\phi+\sigma t)}$, σ being the mode frequency and is

$$4g\Omega(\omega_z + \sigma)\mathcal{I} + \frac{d}{dr} \left(\frac{\mu\Omega}{\sigma - i\alpha_1\Omega + \Omega - \kappa} \frac{dg}{dr} \right) = 0 \quad (18)$$

where $g = v'_z/(\Omega r)$ is the local disc tilt, v'_z being the vertical component of the perturbed velocity. As in paper I the symbols are defined such that

$$\kappa^2 = \frac{2\Omega}{r} \frac{d(r^2\Omega)}{dr} \quad (19)$$

is the square of the epicyclic frequency,

$$\mathcal{I} = \int_{-\infty}^{\infty} \frac{\rho z^2}{c_s^2} dz, \quad (20)$$

$$\mu = \int_{-\infty}^{\infty} \rho z^2 dz. \quad (21)$$

Here it is supposed that the free particle nodal and apsidal precession frequencies $\omega_z = 2S/r^3$, and $\Omega - \kappa = 3\Omega R_+/r - 1.5S/r^3$ are small compared to the unperturbed angular velocity Ω in magnitude.

The relaxation of small amplitude bending disturbances at large radii is described by (18). As in paper I, this occurs through bending waves if $\alpha_1 < H/r$, and through diffusion with diffusion coefficient $\mathcal{D} \sim H^2\Omega/4\alpha_1$ on the characteristic time $t_{diff} = r^2/\mathcal{D}$ at radius r if $\alpha_1 > H/r$. For α_1 not too different from H/r , as in the numerical calculations described here, the relaxation is on the time scale required for bending waves to propagate across the relevant length scale. The waves propagate with speed $c_B = (1/2)\sqrt{\mu/\mathcal{I}} \sim (1/2)H\Omega$, which is one half of a vertically averaged sound speed. The relaxation is towards the solution of (18) corresponding to the least rapid decay in time.

For a disc of infinite extent it is possible to look for a solution of (18) with $\sigma = 0$. This then takes the form

$$g \left(\frac{\Sigma\omega_z}{\Omega} \right) + \frac{d}{dr} \left(\frac{c_B^2\Sigma}{\Omega(-i\alpha_1\Omega + \Omega - \kappa)} \frac{dg}{dr} \right) = 0. \quad (22)$$

When Σ and the disc aspect ratio are asymptotically constant for $r \rightarrow \infty$, (22) has solutions for which g approaches an asymptotically constant value g_∞ such that

$$g \sim g_\infty - g_1 \int_r^\infty \frac{\Omega(-i\alpha_1\Omega + \Omega - \kappa)}{c_B^2 \Sigma} dr, \quad (23)$$

where g_1 is a constant which should be determined according to an appropriate inner boundary condition. As r decreases, one eventually reaches a point where g must begin to depart significantly from its asymptotic value g_∞ . Physically this is because the rate at which the disc is being twisted up by the Lense–Thirring precession begins to dominate over the local propagation/diffusion of disc warp, such that the disc is forced to lie in the equatorial plane of the black hole. We identify the radius where g has to begin to depart significantly from g_∞ with the Bardeen-Petterson transition radius. This radius can be estimated by equating it to the length scale associated with equation (22), or equivalently by the more physical approach of equating the rate at which the disc is twisted up by Lense–Thirring precession with the rate at which warping disturbances are propagated/diffused away. This latter approach is used below. These arguments were also used by Scheuer & Feiler (1996) to derive the transition or warp radius (see their equation (8) and discussion). We comment that the derivation of this transition radius requires the disc to be large in comparison but not necessarily infinite. We emphasise that if the disc is finite but still of significantly greater extent than the transition radius, although some slow long term realignment and precession of the disc will occur due to its finite inertia, the initial relaxation to an approximate steady state like the one considered here is expected. This is in fact borne out by the simulation results.

Scheuer & Feiler (1996) gave a solution of (22) for a constant Σ disc model with constant kinematic viscosity or equivalently, assuming α_1 to be constant, constant c_B^2/Ω . They adopted $\Omega = \kappa$, however their solution can also be extended to the case $(\Omega - \kappa)/\Omega = \epsilon$, with ϵ being constant. The solution for g (which in this context may be identified with the complex conjugate W^* of their function W to within a sign) is then

$$g = g_\infty \exp \left(- \left(\frac{8S\Omega}{c_B^2 r} \right)^{1/2} (-\epsilon + i\alpha_1)^{1/2} \right). \quad (24)$$

As long as $\alpha_1 \neq 0$, this solution is such that $g \rightarrow 0$, for $r \rightarrow 0$.

However, for $\epsilon > 0$, corresponding to prograde precession, as in the Einstein case, and small $|\alpha_1/\epsilon|$, the solution exhibits many wavelike oscillations which may be interpreted as *inward* propagating bending waves excited in the transition region. This is in contrast to the situation of retrograde precession, $\epsilon < 0$, as in the softened case, where the waves are evanescent. This phenomenon has been already noted by Ivanov & Illarianov (1997) and, as we shall see, it has some consequences for the calculation of the torque exerted between the black hole and disc in the limit of small α_1 . But note that solutions with many oscillations in the inner disc appear in a linear theory. It is likely that non-linear effects are likely to make very short wavelength waves disappear.

The case of Einstein precession has $\epsilon = 3R_+ / r$, which is not constant. However a solution of the Scheuer & Feiler (1996) type may be found in this case for constant Σ in the limit of vanishing α_1 , if we assume the kinematic viscosity or equivalently $c_B^2/\Omega \propto 1/r$. This is

$$g = g_\infty \exp \left(-i \left(\frac{24SR_+\Omega}{c_B^2 r} \right)^{1/2} r^{-1/2} \right). \quad (25)$$

5 THE TRANSITION RADIUS

In order to obtain an estimate of the transition radius for the warp, we need to equate the rate at which the disc is twisted up by the rate at which warping disturbances are propagated across the disc. We note that estimates of the transition radius based on this approach should provide results that are accurate to within a factor of order unity. The physical processes of twisting the disc up and propagating/diffusing the warp occur over a range in radii such that the transition between aligned and misaligned planes will also occur over a range in radii, rather than at a single location. In the diffusive limit where $H/r < \alpha_1$, and $\alpha_1 > |\Omega - \kappa|/\Omega$, we equate the rate of twisting up by differential precession and the rate of diffusion of warps. The rate at which the disc is twisted up is given by $1/\tau_{dp} = |r(d\omega_z/dr)| = 6S/r^3$. In the diffusion limit, the warping of the disc is counteracted by diffusion of the warp, which acts at a rate $1/t_{diff}$ where $t_{diff} = r^2/\mathcal{D}$ and $\mathcal{D} = c_B^2/(4\alpha_1\Omega)$ is the diffusion coefficient. Equating these two rates leads to an expression from which the transition radius can be found:

$$R_{T1} = \left\{ \frac{24\alpha_1 S}{\sqrt{GM}} \left(\frac{H}{r} \right)^{-2} \right\}^{2/3} \quad (26)$$

This should be contrasted with the expression for the transition radius, R_{BP} , obtained using thin disc theory in which the effects of pressure forces are neglected and an isotropic viscosity is assumed (Bardeen & Petterson 1975; Hatchet, Begelman, & Sarazin 1981):

$$R_{BP} = \left\{ \frac{6S}{\alpha\sqrt{GM}} \left(\frac{H}{r} \right)^{-2} \right\}^{2/3}. \quad (27)$$

Here α is the standard viscosity parameter associated with the radial accretion. It is apparent that if $\alpha \ll 1$, then $R_{BP} \gg R_{T1}$ and the transition radius predicted by (27) will lie much further away from the black hole, with the warp extending over a much greater proportion of the accretion disc than when (26) is used. This arises because the viscous damping of the resonantly driven horizontal motions included when (26) is used leads to a larger diffusion coefficient, and thus to a more rapid damping of the warp.

It should be noted that R_{T1} given by (26) continues to decrease as α_1 decreases. Here we remark that for a strictly Keplerian disc the diffusive behaviour of warps used in (26) requires for its validity that $\alpha_1 > H/r$. When $\alpha_1 \sim H/r$, warps are diffused across the disc on essentially the sound crossing time. At the beginning of the transition to the wave communication regime, we replace α_1 by H/r in (26), giving a second estimate of the transition radius

$$R_{T2} = \left\{ \frac{24S}{\sqrt{GM}} \left(\frac{H}{r} \right)^{-1} \right\}^{2/3}. \quad (28)$$

Note further that the disc is not strictly Keplerian in which case apsidal precession, which inhibits the communication of warps, should be taken into account. This modifies (26) for the diffusive regime to provide a third estimate of the transition radius.

$$R_{T3} = \left\{ \frac{24S\sqrt{(\alpha_1^2\Omega^2 + (\Omega - \kappa)^2)}}{\Omega\sqrt{GM}} \left(\frac{H}{r}\right)^{-2} \right\}^{2/3}. \quad (29)$$

Note that if we take account of the fact that $\Omega \neq \kappa$, because $S \neq 0$, but ignore the effect of Einstein precession, then we recover (28) in the limit of small α_1 .

The above discussion suggests that to estimate the Bardeen-Petterson radius we should take the maximum value found from using (26), (28) or (29). In this way unrealistic efficiency in warp communication is avoided. However, we remark that the transition radius is expected to be many gravitational radii from the black hole justifying the post Newtonian approximations in estimating its location. We further remark that the appropriate values of α_1 for our disc models were calibrated using calculations similar to those presented in paper I and those in Nelson, Papaloizou, & Terquem (1999). These values are given in the introduction.

6 NUMERICAL METHOD

The set of fluid equations described in section (2) are solved using smoothed particle hydrodynamics (Lucy 1977; Gingold & Monaghan 1977). The SPH code used to perform the calculations presented in this paper is identical to that used in paper I, and we refer readers to this paper and references therein for a description of our numerical scheme.

7 CALCULATIONS OF THE BARDEEN-PETTERSON EFFECT

We have performed a number of calculations to examine the structure of an accretion disc produced when in orbit about a Kerr black hole, with the effects of Lense-Thirring precession included in the equations of motion. The calculations assume that the angular momentum vectors of the disc material and the spinning black hole are initially misaligned by some amount, with the system being evolved until a quasi steady state is achieved. The main issue that we wish to address in these simulations is the location of the so-called ‘Bardeen-Petterson radius’. This is the region of transition in the disc between the inner part, which in a steady state is expected to lie in the equatorial plane of the black hole due the combined effects of differential precession and viscosity, and the external part which is expected to remain in its original plane if the disc is effectively infinite. Due to the limitations of computational tractability, we are only able to consider discs which are of finite size. We do not expect this to affect the results on the transition radius, provided that the outer disc radius is sufficiently far from the transition zone, as is the case in our disc models. The initial conditions of each of the calculations were varied, such that the effects of changing the disc thickness, the exact form of the central potential, the number of particles, the disc radius, and the inclination angle between the black hole equator and initial disc midplane could be studied. These initial conditions are described in detail in the following section, which is followed by a description of the results from the numerical calculations.

7.1 Initial Conditions

In each of the Bardeen-Petterson calculations, the central mass $M = 1$, the gravitational constant $G = 1$, $a = 1$, and $\mathbf{S} = 0.008$ in equation (4). This leads to a value of the gravitational radius of $R_+ = 0.04$ in our computational units. The calculations can be divided essentially into two groups, those in which the central Keplerian potential was softened, and those in which no softening was used but in which the effects of Einstein precession were included. We will describe the former group of calculations first, followed by the latter group. One additional calculation was performed in which the effects of Einstein precession were neglected and no softening of the central potential was used, leading to a disc with a Keplerian rotation profile. All calculations are presented in table 1, with the predicted value of R_{T2} from equation (28) being shown in the eighth column, and that measured from the SPH calculations, R_{TS} being presented in the last. In this paper we define R_{TS} , the transition radius measured from the simulations, to be the radius at which the disc tilt has a value that is half way between that of the inner and outer parts of the relaxed warp disc models, unless otherwise stated.

The gravitational softening parameter used in equation (7) was $b = 0.2$. A number of disc models were employed to examine the Bardeen-Petterson effect. An initial calculation used a disc model of radius $R = 1$ and employed $N = 20,000$ particles. This calculation had a midplane Mach number of $\mathcal{M} \simeq 12$. Two calculations were performed with disc models of radius $R = 2$ and with $N = 52,000$. These calculations had $\mathcal{M} \simeq 12$ and 30 respectively. Two calculations were performed with a disc of radius $R = \sqrt{2}$ and $N = 102,000$ particles, one with $\mathcal{M} \simeq 9$, and the other with $\mathcal{M} \simeq 12$. An additional calculation was performed with $R = \sqrt{2}$, $N = 60,000$, and $\mathcal{M} \simeq 12$. In all cases, the inclination between the black hole equator and the initial disc midplane was $i = 10^\circ$.

The calculations in which no gravitational softening was employed, and which included the effect of Einstein precession, had the central black hole treated as a uniform density sphere of finite size ($b = 0.2$) in order to prevent numerical divergences as the disc material extends towards $r \rightarrow 0$. Six calculations of this type were computed overall. Five of them had $R = 2$ and $N = 52,000$, two of which had had $i = 10^\circ$ and $\mathcal{M} \simeq 12$ and 30, two of which had $i = 30^\circ$ with $\mathcal{M} \simeq 12$ and 30, and one had $i = 10^\circ$ and $\mathcal{M} = 5$. The sixth calculation had $i = 10^\circ$, $R = 7$, $N = 200,000$, and $\mathcal{M} \simeq 14$. An additional calculation was performed in which the effects of Einstein precession were neglected and no softening of the gravitational potential was used. This calculation had $i = 30^\circ$, $\mathcal{M} = 12$, $R = 2$, and $N = 52,000$, and was performed to provide a comparison case with the other high inclination runs.

All calculations were initiated with the disc orbiting the black hole, and with the inclination between the black hole equator and the *original* disc plane being constant throughout the calculations. The calculations were all evolved towards a quasi steady state, such that a precessing, but otherwise almost stationary warped structure was obtained in each case. The results of these calculations are described in the following section.

Run	i	R	\mathcal{M}	b_{soft}	Ein Prec?	N ($\times 10^3$)	R_{T2}/R_+	R_{TS}/R_+	t_{run}/τ_{dp}
S1	10	1	12	0.2	No	20	43	17	2.4
S2	10	2	12	0.2	No	52	43	16	2.4
S3	10	$\sqrt{2}$	12	0.2	No	60	43	16	2.1
S4	10	$\sqrt{2}$	12	0.2	No	102	43	16	2.4
S5	10	$\sqrt{2}$	9	0.2	No	102	33	10	14
S6	10	2	30	0.2	No	52	80	33	2
E1	10	2	12	0	Yes	52	43	14	2.6
E2	10	2	30	0	Yes	52	80	28	2.9
E3	30	2	12	0	Yes	52	43	20	5
E4	30	2	30	0	Yes	52	80	25	5
E5	10	2	5	0	Yes	52	24	0	-
E6	10	7	14	0	Yes	200	48	19	2.4
K1	30	2	12	0	No	52	43	23	5

Table 1. The first column provides the label given to each run, the second column provides the initial inclination. The third column gives the disc radius, and the fourth column gives the midplane Mach number of the disc model. The fifth column gives the gravitational softening length, the sixth column indicates whether or not Einstein precession was included, and the seventh column gives the number of particles used. The eighth column gives the predicted value of the transition radius from equation (28), and the ninth column gives the value of the transition radius measured from the simulations, in units of the gravitational radius. The last column provides the time over which the simulations were run in terms of the differential precession time at the outer edge of the transition zone.

8 RESULTS

In this section we present and discuss the results of the calculations described in section (7.1). The results of the calculations that were performed using a softened gravitational potential are described first, followed by the calculations in which the effects of Einstein precession were included.

In the discussion of the results that follows, we will be describing the evolution of the angle of inclination between angular momentum vector of the black hole, \mathbf{J}_{bh} , and the specific angular momentum vector of the disc material, \mathbf{J}_d . This quantity is defined through the expression

$$i(r) = \arccos \left(\frac{\mathbf{J}_{bh} \cdot \mathbf{J}_d(r)}{|\mathbf{J}_{bh}| |\mathbf{J}_d(r)|} \right), \quad (30)$$

and may be a function of radius through the disc, such that the disc is warped. The calculations are initiated with this quantity being constant throughout the disc. We note that g , introduced in equation (18), and i are equivalent. We will also be describing the precession of the local angular momentum vector in the disc, projected onto the fixed x - y plane of the black hole equator. This precession angle is defined by the expression

$$\beta(r) = \arccos \left(\frac{\mathbf{J}_{bh} \times \mathbf{J}_d(r)}{|\mathbf{J}_{bh} \times \mathbf{J}_d(r)|} \cdot \hat{\mathbf{y}}_o \right), \quad (31)$$

and may vary as a function of radius in the disc, such that the disc is twisted. Here, $\hat{\mathbf{y}}_o$ is the unit vector pointing in the y direction located in the fixed equatorial plane of the black hole. The calculations are initiated with $\beta = \pi/2$ throughout the disc.

The results shown in the particle projection plots are presented in a fixed reference frame centred on the black hole. The initial inclination between the disc midplane and the black hole equator is provided by rigidly rotating the disc about a diameter coincident with the x axis in this fixed reference frame.

The evolution of all of the disc models in the simulations is as follows. Initially, there is a short period of rapid evolution during which the inner parts of the disc undergo strong differential precession and are forced to lie in the symmetry plane of the black hole out to a transition region, beyond which the discs remain in their original plane. During this time, warping disturbances propagate through the disc either as bending waves or through diffusion, and a warped disc configuration is set up on the time scale required for these warps to propagate across the disc. This time scale for the the warped configuration and the transition zone to be

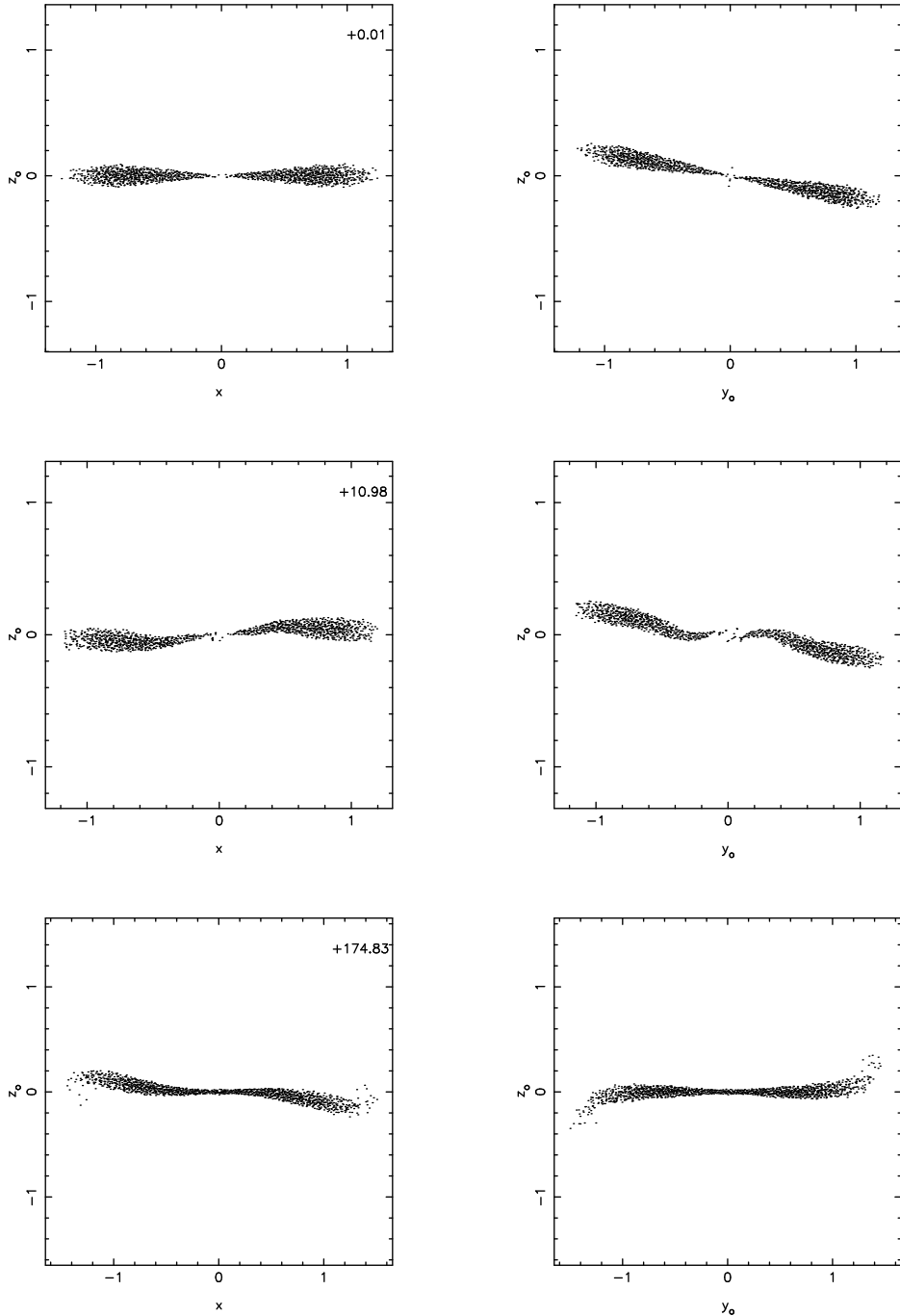


Figure 1. This figure shows particle projections of cross sectional slices through the disc in calculation S1. The time is shown in units of $\Omega(R = 1)^{-1}$ in the top right corner of each left hand panel.

set up also corresponds to the differential precession time scale measured at the transition radius, τ_{dp} . The discs were all evolved for a time $\gg \tau_{dp}(R_{TS})$ to ensure that the position of the transition zone had been firmly established. The run time of each calculation, in terms of the relevant differential precession time τ_{dp} , is given in table 1. There then follows a period of evolution that occurs on a much longer time scale involving near-rigid body precession of the disc, and a slow alignment of the outer parts of the disc with

the symmetry plane of the central black hole. This period of evolution arises because of viscous coupling between the misaligned inner and outer parts of the disc, and as a result of residual torquing by the black hole beyond the transition radius. It does not arise because warping disturbances are being propagated to large radii from within the transition zone of the disc. The communication of warps by bending waves or diffusion appears to be confined within the transition zone, exactly as expected from the linear theory. This

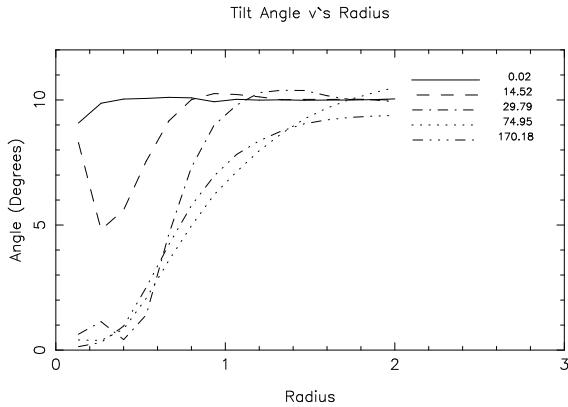


Figure 2. This figure shows the evolution of disc tilt as a function of radius for the calculation S2, with midplane mach number $\mathcal{M} \simeq 12$.

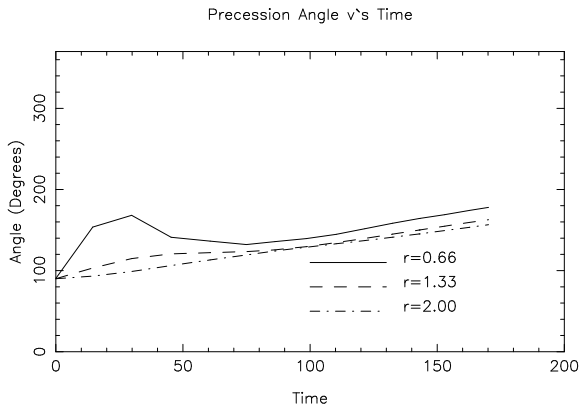


Figure 3. This figure shows the precession angle as a function of time for three different disc annuli in calculation S2. Note the initial differential precession which relaxes towards near solid body precession after $t \simeq 100$. The outer radius of each annulus is indicated in the figure panel.

is evidenced by the fact that the outer regions evolve much more slowly than they would if they were being torqued into alignment as a result of warps propagating from the inner regions of the disc. We have examined the outer parts of the discs in our models, and find no evidence of warping disturbances reaching them from their central parts over time scales that are typically \sim few hundred $\Omega(R=1)^{-1}$. We interpret this to mean that using disc models with larger outer radii will not result in changes to the locations of the transition radii that we find in our models. This is confirmed by run E6.

8.1 Calculations Employing Gravitational Softening

A number of calculations were performed in which the central gravitational potential was softened and the effects of Einstein precession were neglected. These calculations were performed with $\mathcal{M} \simeq 9, 12$ or 30 (*i.e.* with $H/r \simeq 0.11, 0.08$ or 0.03).

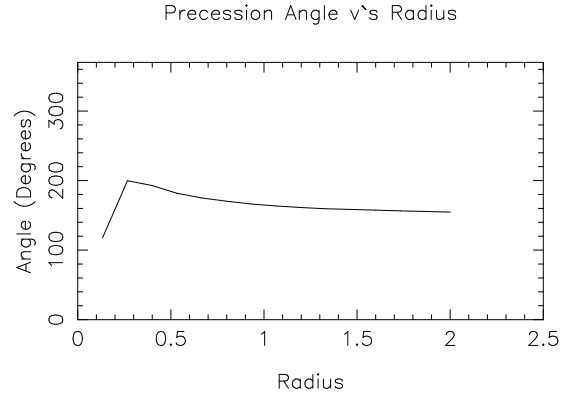


Figure 4. This figure shows the degree of twist in the disc at the end of calculation S2. Note that the inner disc is twisted relative to the outer disc by an angle of ~ 25 degrees.

8.1.1 $\mathcal{M} \simeq 12$ Calculations

A time sequence showing the evolution of calculation S1, listed in table 1, is shown in Fig. (1). Projections of particles contained within a thin slice centred about the x axis (left panels) and the y axis (right panels) are presented, with the time corresponding to the panels being shown in units of Ω^{-1} at $R=1$ in the top right hand corner of the left hand panels. The top two panels show the disc at the beginning of the calculation, with the initial tilt of the disc relative to the fixed coordinate system being apparent in the right hand panel. As the calculation proceeds, the Lense–Thirring precession twists up the inner parts of the disc, which are forced eventually to lie in the equatorial plane of the black hole, with the outer disc remaining close to its original plane. The middle two panels show the disc at an intermediate state of its evolution, during the time in which the inner parts of the disc are still in the process of flattening out into the equatorial plane of the black hole. The final two panels show the disc after it has evolved towards a quasi–steady state configuration, in which a smoothly varying warped disc has been established which undergoes approximate solid–body precession. We comment that this non zero precession rate is a consequence of having a finite disc. If the disc were to extend to arbitrary large radii, the angular momentum content may tend to arbitrary large values while the total mass remained finite. Then the precession period would approach arbitrary large values.

Fig. (2) shows the time evolution of the disc tilt versus radius for the calculation S2 shown in table 1, with the unit of time being Ω^{-1} evaluated at $R=1$. The angular momentum vector of the disc at each radius is initially tilted by $i = 10^\circ$ with respect to the angular momentum vector of the black hole. As the calculation proceeds the inner parts of the disc begin to lie in the equatorial plane of the black hole, and eventually a disc configuration is developed in which the disc tilt varies smoothly as a function of radius, and with the radius of transition between the inner and outer planes being at around $R_{TS} \sim 0.6$, which is equivalent to $R_{TS} = 15 R_+$ in our units. To recap, we define the transition radius measured in the simulations, R_{TS} , to be the radius at which the disc angle of tilt is half way between that of the outer part of the disc and the inner part of the disc. In

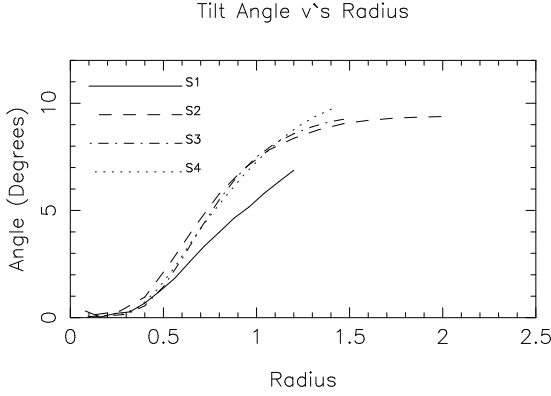


Figure 5. This figure presents a comparison of tilt profiles obtained in calculations S1, S2, S3, and S4 which each had mid-plane Mach number of $\mathcal{M} \simeq 12$. Note that each calculation produces a fully aligned region of the disc that extends out to $R \simeq 0.4 = 10R_+$.

the case of calculation S2, the transition zone approximately occupies the range of radii 0.4 – 1.5. The differential precession time measured at $R = 1.5$ is $\tau_{dp}(1.5) = 70 \Omega(R = 1)^{-1}$. The calculation is evolved for $170 \Omega^{-1}$ without any apparent change in the transition radius between the times 100 – 170 Ω^{-1} . We find in this calculation, and in the others also, that the position of R_{TS} agrees reasonably well with the semi-analytic formulae presented in section 4, such as equation (28), to within a factor of 2 or 3, thus justifying the physical arguments leading to these expressions. We note that the choice of defining R_{TS} to be the radius corresponding to the half way point of the warped region is somewhat arbitrary, and that a definition of R_{TS} being the position where the inclination approaches its value at the outer disc edge would produce values of R_{TS} in table 1 that are in greater agreement with the tabulated values of R_{T2} . We also comment that the inclination of the outer disc boundary is free, and thus its location should not affect the position of the transition radius if it is sufficiently distant (compare models S1, S2, S3, S4 in Fig. [5], and E6 in Fig. (13). The equations (26), (28), and (29) that predict the transition region were derived under the assumption of linearity of the warp. We note that the warp in the Mach 30 cases is nonlinear, as described in paper I, such that we should expect a poorer agreement between the transition radii measured in the simulations and those predicted using equations such as (28).

Fig. (3) shows the time evolution of the nodal precession angle, β , for different annuli of the accretion disc, computed from the results of calculation S2. The definition of β is given by equation (31), such that at time $t = 0$, $\beta = 90^\circ$ for the whole disc. In Fig. (3), the disc has been subdivided into three annuli which each lie in the range $0 \leq r < 0.66$, $0.66 \leq r < 1.33$, and $1.33 \leq r \leq 2$, respectively. As the calculation proceeds, it may be observed that the disc initially undergoes a period of differential precession, with the inner disc precessing more rapidly than the outer disc, before settling down to a quasi steady state in which the disc precesses approximately as a rigid body. The degree of twist in the disc at the end of the calculation is represented in Fig. (4). This figure indicates that the angle between the

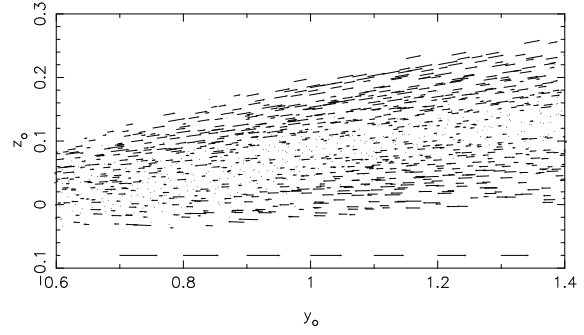


Figure 6. This figure shows the vertical shearing motion generated in the warped accretion disc modeled in calculation S4. This shearing motion is observed in all models in the regions of the disc where the curvature, $\partial g/\partial r$, is non zero.

line of nodes of disc annuli in the inner part of the disc, say at $r = 0.6$, and the outer disc edge is $\sim 25^\circ$, showing that the disc has developed a $\sim 25^\circ$ twist before reaching a quasi equilibrium state.

A comparison between each of the runs with midplane Mach numbers $\mathcal{M} \sim 12$ is presented in Fig. (5). This figure shows the results from each of the runs S1, S2, S3, and S4 presented in table 1. It is apparent that the radial variations in tilt, and in particular the positions of the transition radii, are similar in each case, even though the resolution of each calculation differs, indicating that convergence of the results has been attained. We note that the position of outer radius of the disc does not seem to alter the location of the transition region, since the outer disc lies sufficiently beyond the warped region. The curve corresponding to the $R=1$ disc (calculation S1) shows that the outer parts of this disc are tending towards alignment with the black hole equatorial plane. This is expected for all discs of finite extent, and hence finite angular momentum and moment of inertia, since there is a torque between the inner and outer parts of the disc that attempts to bring them into alignment. The rate at which this occurs obviously depends on the angular momentum content, and hence radius, of the disc, with a smaller disc being aligned more quickly. The larger ($R = \sqrt{2}$ and $R = 2$) discs will also eventually evolve towards alignment, but on a time scale that is longer than the time for which these calculations were run. This issue will be discussed in greater detail in section 8.5.

As described in paper I, the result of warping a vertically stratified, gaseous accretion disc is to set up vertical shearing motions, such that the perturbed radial velocities, v_r , are an odd function of z . The warped discs generated by the action of Lense–Thirring precession indeed show such a kinematic feature over those portions of the disc where the inclination, i , varies with radius. This fact is illustrated by Fig. (6), in which the radial velocities of the particles contained within a thin slice of the disc centred about the y axis are represented by velocity vectors. The arrows located at the bottom of the figure indicate the magnitude of the midplane sound speed at each position. The data used to generate this figure were obtained from the calculation S4.

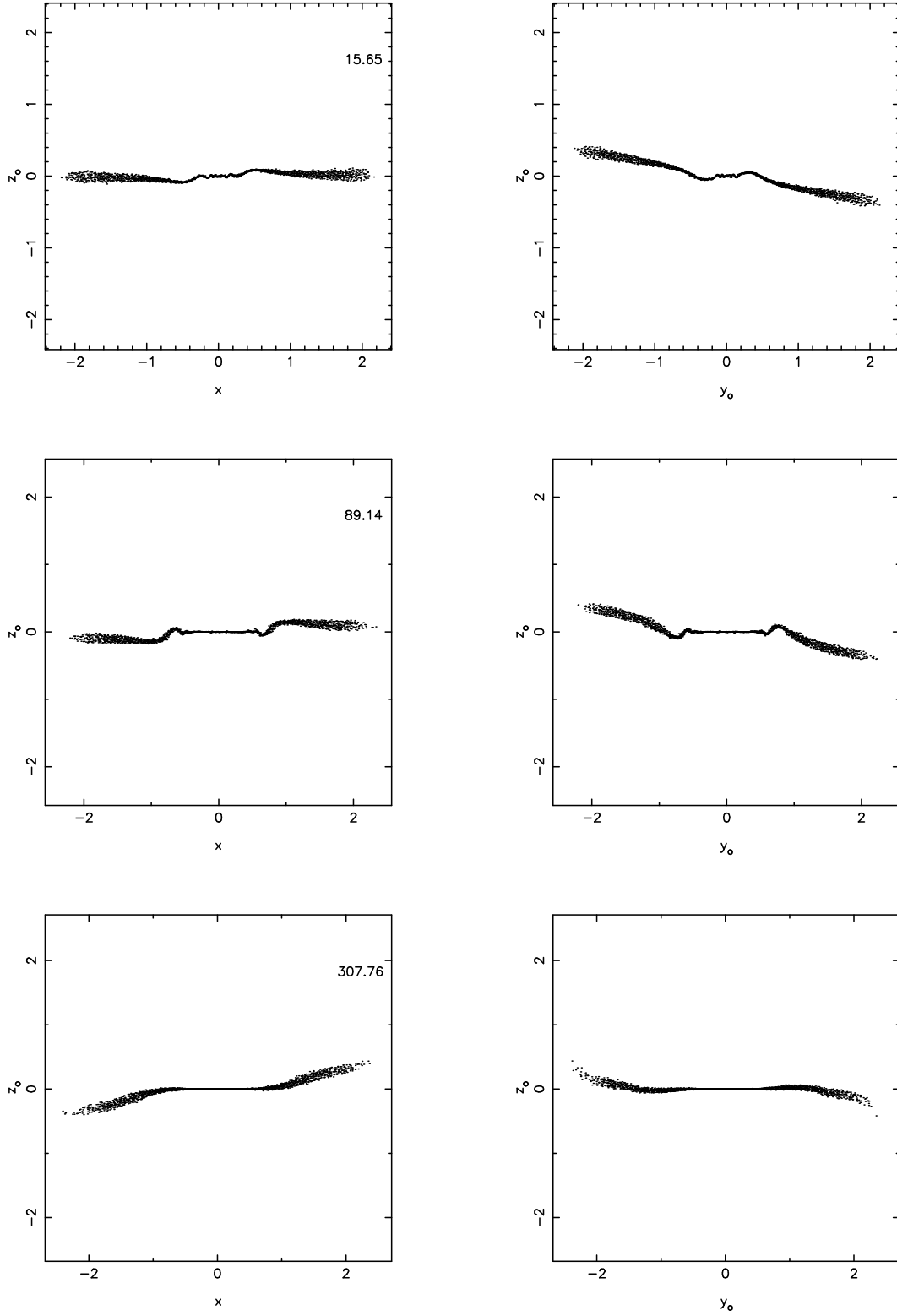


Figure 7. This figure shows particle projections of cross sectional slices through the disc in calculation S6. The time is shown in units of $\Omega(R = 1)^{-1}$ in the top right corner of each left hand panel. Note that the ‘wiggles’ observed in the disc are transient, and damp out by the end of the calculation.

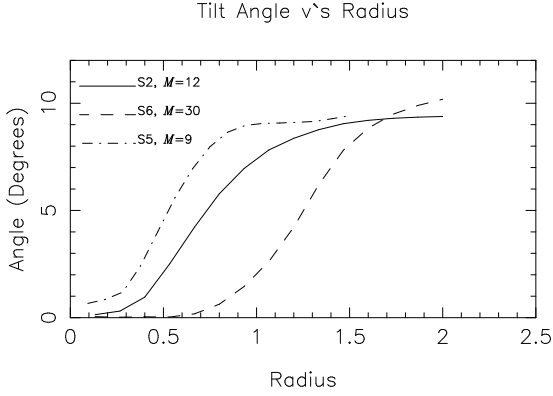


Figure 8. This figure shows the variation of disc tilt with radius at the end of the calculations S2, S5, and S6. The value of the Mach number at the disc midplane is given in the figure panel alongside the figure labels. Note that the transition radius R_{TS} moves in as the midplane Mach number is decreased.

8.1.2 Changing the Disc Thickness – $\mathcal{M} \simeq 30$ and $\mathcal{M} \simeq 9$ Calculations

A time sequence showing the evolution of the disc during the calculation S6 is shown in Fig. (7). Projections of particles contained within a slice centred about the x axis (left panels) and the y axis (right panels) are presented. The time corresponding to each panel is shown in the top right hand corner of each left hand panel in units of Ω^{-1} evaluated at $R = 1$. The first two panels show the disc after it has evolved for $t \simeq 15 \Omega^{-1}$, and the existence of apparent ‘wiggles’ may be observed in the inner parts of the disc. These features are transient phenomena and are caused by the differential precession of the inner disc. As time proceeds, the wiggles damp away, as the inner disc flattens into the equatorial plane of the black hole, eventually leaving a disc with a warp that is slowly varying as a function of radius. We notice that the inner region of the disc that becomes aligned with the black hole equator is of much greater radial extent than that occurring in Fig. (1), as expected from the discussion presented in section 4.

The variation of disc tilt as a function of radius is plotted for three different runs in Fig. (8) in order to examine the effect of changing the disc thickness. The midplane Mach number of each run is $\mathcal{M} \sim 9$ (*dot-dashed* line), $\mathcal{M} \sim 12$ (*solid* line), and $\mathcal{M} \sim 30$ (*dashed* line), and it is apparent that the transition radius increases with increasing \mathcal{M} . This result is expected from the analytic estimates of R_{T1} and R_{T2} presented in section 4, since a thicker disc diffuses disc warp more efficiently. The value of R_{TS} changes from $R_{TS} \sim 10R_+$ to $16R_+$, and $33R_+$ as \mathcal{M} changes from $\mathcal{M} \sim 9$, 12, and 30, respectively. It should be noted that these values of R_{TS} are very much smaller than those predicted using the thin viscous disc theory neglecting hydrodynamical effects, (Bardeen & Petterson 1975), and confirm the previous assertions of Papaloizou & Pringle (1983), and Kumar & Pringle (1985), that taking into account the full disc hydrodynamics results in a transition radius that lies much closer to the central black hole.

The degree of twist in the $\mathcal{M} \sim 30$ disc is shown in Fig. (9), and indicates that the twist angle between the line

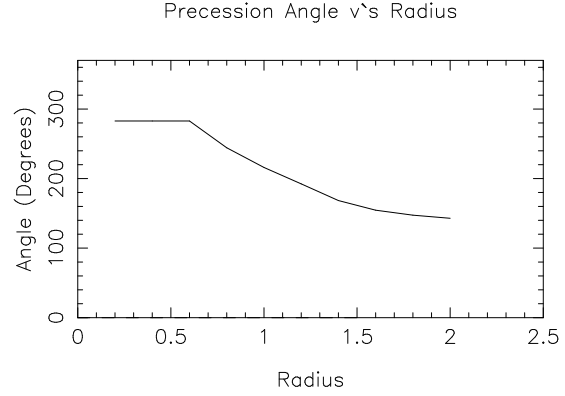


Figure 9. This figure shows the degree of twist in the disc at the end of calculation S6, which has a midplane Mach number of $\mathcal{M} \simeq 30$. Note that the inner disc is twisted relative to the outer disc by an angle of ~ 90 degrees, which should be contrasted with that in calculation S2, where $\mathcal{M} \simeq 12$.

of nodes in the inner ($R \sim 0.9$) and outer parts ($R = 2$) of the disc is $\sim 90^\circ$, which is significantly larger than was found to be the case for the $\mathcal{M} \sim 12$ disc. This larger twist occurs because communication through the disc by bending waves/diffusion is much less efficient in this case, so that the disc needs to acquire a more distorted configuration before it can obtain a quasi steady state structure which undergoes approximate solid body precession.

We note that although the numerical resolution in the $\mathcal{M} \sim 30$ calculations is reduced relative to the $\mathcal{M} \sim 12$ calculations, a plot of the velocity field similar to that shown in Fig. (6) produces a similar picture of a disc in which the vertical shearing motion extends over those regions of the disc in which i , the disc inclination, varies with radius (*i.e.* in those regions where the curvature of the disc is non-zero). We also found that these motions were subsonic which is consistent with the idea that damping due to shocks keeps them down to this level. This indicates that the thinner disc models still have their vertical structure modeled to a reasonable degree of accuracy, such that it is able to produce this vertical shear. This is because the smoothing lengths still remain $< H$, the disc semi-thickness, beyond that region of the disc which resides in the equatorial plane of the black hole, and where it becomes noticeably curved.

We remark that calculation E5, which has the largest disc thickness of the models we considered with $\mathcal{M} = 5$, showed no signs of alignment in its inner regions, and represents the limiting disc thickness that allows the formation of a noticeably warped disc. This has relevance to the properties of the thick advection dominated accretion discs (*i.e.* ADAFs) around rotating black holes, which will presumably show no outward signs of being warped.

8.2 Calculations Including the Effects of Einstein Precession

The discussion of warp propagation given in paper I indicates that efficient, non dispersive bending wave propagation is expected to occur only for Keplerian accretion discs in which $\Omega \simeq \kappa$. In a situation where $\Omega \neq \kappa$, then the com-

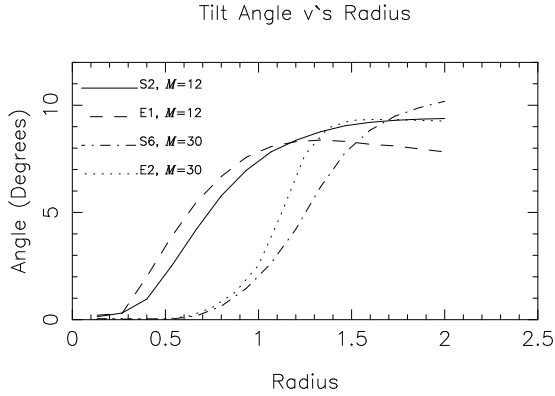


Figure 10. This figure shows the effects of including Einstein precession on the variation of disc tilt with radius. The calculations E1 and E2 have sharper transitions between the inner outer disc relative to their softened counter parts S2 and S6.

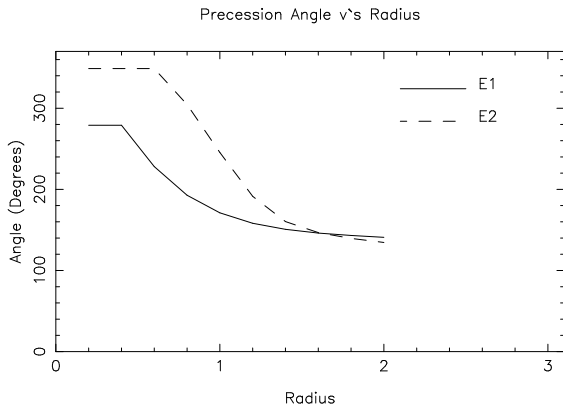


Figure 11. This figure shows the degree of twist in the discs at the end of calculations E1 and E2. Note that the inner disc is twisted relative to the outer disc by an angle of $\sim 90^\circ$ in calculation E1, and by $\sim 120^\circ$ in E2, which should be contrasted with the twist in the calculations with gravitational softening S2 and S6.

munication of warping disturbances is expected to become dispersive, with the effects of this dispersion becoming more important as $|\Omega - \kappa|$ increases (*i.e.* as the apsidal precession frequency increases), since the resonance between the circular and epicyclic motion becomes increasingly detuned. As was noted in section (3), the frequency of Einstein precession (*i.e.* advance of periape) remains relatively high out to quite large radii in our disc models, indicating that it may be an important consideration in determining the structure and evolution of warped accretion discs around black holes.

A comparison between the calculations S2 and E1 is presented in Fig. (10). The *solid* line shows the variation of disc tilt versus radius for calculation S2, whereas calculation E1 is indicated by the *dashed* line. The primary difference between the cases with Einstein precession included and those with it neglected is that the transition between the inner and outer disc planes occurs much more sharply when Einstein precession is included. The calculations for $i = 10^\circ$ and $\mathcal{M} = 30$ are also shown in Fig. (10), S6 being shown by

the *dashed-dotted* line and E2 by the *dotted* line, and illustrate this steeper transition between the inner and outer disc planes more clearly. This arises because the communication of the disc tilt between the two misaligned planes is more effective when Einstein precession is neglected, so that the transition may be smoothed out more effectively by the enhanced diffusion of disc tilt.

One effect of this modification of disc structure by the inclusion of Einstein precession in our calculations is to change the rate at which the outer disc tends to align with the equatorial plane of the black hole. The existence of a more discontinuous transition between the two disc planes leads to a larger frictional/viscous interaction between the outer and inner disc at their points of intersection, and thus to a larger torque that acts to realign the two separate regions of the disc. Since the inner disc is anchored to the black hole equatorial plane by the Bardeen–Petterson effect, the outer disc is also forced to evolve towards this plane. Our calculations indicate that this rate of realignment is enhanced when Einstein precession is included. Although this seems counter intuitive since disc tilt is supposed to diffuse through the disc at a lower rate when the rotation profile is non Keplerian, this result is in agreement with the predictions of linear theory, as discussed in section (8.5).

In addition to the transition between the inner and outer disc planes being steeper, we also find that the disc twist is greater when Einstein precession is included. Fig. (11) shows the precession angles of different disc annuli at the end of the calculations E1 and E2. These plots should be compared with Figs. (4) and (9) which show the precession angles for the calculations S2 and S6. We find that calculation E1 results in a twist of the disc of $\sim 90^\circ$ between the radii $R = 0.6$ to 2.0 , which should be compared with $\sim 25^\circ$ for calculation S2. A similar comparison between E2 and S6 yields twist angles of $\sim 120^\circ$ and 90° , respectively. This is entirely consistent with linear analysis [see section (8.5)] which indicates that inward propagating short wavelength bending waves should be present in the inner part of the transition region producing a twist there. Physically the large twist angles produced in the simulations are a result of the diminished efficacy of communication between neighbouring annuli in the disc when the rotation profile becomes significantly non Keplerian. In order for such a disc to settle to a steady state structure which is in a state of near solid body precession, the disc must become more severely distorted and twisted so as to increase the torques acting between neighbouring annuli of gas.

We remark that many oscillations in disc tilt as indicated by the linear analysis discussed here and found in the linear calculations of Ivanov & Illarianov (1997), do not appear in our nonlinear simulations. This is presumably because non linear effects lead to the damping of these short wavelength features, and alignment of the inner disc regions in which the tilt amplitude would otherwise change rapidly on small length scales.

8.3 Effects of Increasing the Inclination Angle i

Three calculations were performed with larger degrees of inclination between the black hole equatorial plane and the original disc plane. These were the calculations listed as E3, E4, and K1 in table 1 .

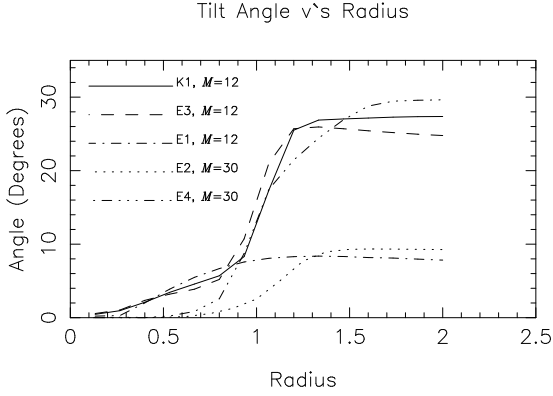


Figure 12. This figure shows the variation of disc tilt with radius for the high inclination runs E3, E4, and K1. Also plotted are the tilt variations calculated in the models E1 and E2 for comparison purposes. Note that the misaligned inner and outer disc parts occupy a similar radial extent when going from low to high inclination, leading to a sharp transition in the high inclination cases.

The results of these calculations are plotted in Fig. (12), along with those of calculations E1 and E2 which are plotted for the purpose of comparison. As in the previous runs, the calculations result in a disc structure which is essentially composed of two mutually inclined regions, the inner and outer disc, and a transition zone between them. In the low inclination ($i = 10^\circ$) runs, the transition zone appears to join the two misaligned inner and outer disc parts more smoothly than is the case with the higher inclination ($i = 30^\circ$) runs. This is because the inner disc, which becomes aligned with the black hole equator, and the outer disc, which remains in its original plane, occupy approximately the same intervals in radius irrespective of whether the inclination angle is 10° or 30° . Thus, the transition between these two planes occurs more steeply simply because of the greater degree of inclination when $i = 30^\circ$. The steepness of the transition in the 30° inclination degree runs, combined with an inspection of the disc structures resulting from the calculations E3 and E4, indicate that the discs are close to breaking into two discrete pieces with only a tenuous bridge of material connecting them. The dominant means by which the two separate pieces of the disc communicate with one another is probably through the viscous coupling at their region of intersection rather than through wave-like or diffusive communication.

8.4 A Larger Disc Model

A calculation was performed using a disc model with an outer radius at $r = 7$ in order to ensure that the transition radii obtained in previous sections are not affected by the smaller disc models used. This calculation is listed as run E6 in table 1, and employed 2×10^5 particles. The midplane Mach number $\mathcal{M} \sim 14$, and the expected value of $\alpha_1 \sim 0.04$, so that bending waves are expected to travel in this disc model. The effects of Einstein precession were included so that equation (8) was used to calculate the gravitational force.

The evolution of the disc tilt for this run can be observed

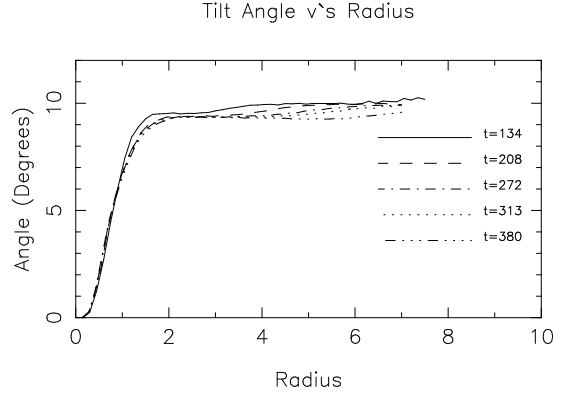


Figure 13. This figure shows the time variation of disc tilt with radius for the large disc model E6 with outer radius at $r = 7$ described in the text. It is apparent that the transition radius is essentially set up after $t \sim 134$ with some additional relaxation occurring up to $t \sim 208$. We note that the differential precession time at $R = 2$ is $\tau_{dp} = 166$. After this time the transition radius remains fixed, with the disc outside of this radius being slowly torqued into alignment with the equatorial plane of the black hole.

in Fig. (13) where each line corresponds to the disc tilt versus radius at different times during the run. The times are shown in the figure in units of Ω^{-1} evaluated at $R = 1$. We note that the warped disc and the transition radius are expected to be set up after a time corresponding to the differential precession time at the radius of the transition zone. From Fig. (13) we notice that the transition radius, as defined in the first paragraph of section 7.1, is located at $R \sim 0.77 = 20R_+$, with the disc tilt approaching that of the original disc beyond a radius of $r \sim 2$. This result agrees very well with those obtained for the disc models with $\mathcal{M} \sim 12$ and outer radii of $r = 2$ described in previous sections, as seen in table 1. The larger disc of radius $r = 7$ is slightly thinner with $\mathcal{M} \sim 14$, with the result that the transition zone is slightly further out in this case. The differential precession time at a radius of $r = 2$ is $\tau_{dp} \simeq 166$, which is the time required for the transition zone to become fully relaxed. The calculation ran for a time of $\sim 400 \Omega(R = 1)^{-1}$. It is apparent that once the transition zone has been established on the precession time, its position remains fixed when the calculation is continued for a number of precession times. The disc exterior to the transition zone undergoes some longer time scale readjustment as a transient disturbance propagates through the disc from the central regions. As is the case with the calculations presented in previous sections, the outer disc undergoes a process of slow realignment with the black hole equator, with the location of the transition radius remaining fixed throughout this period of the evolution.

Particle projection plots are presented in Fig. (14) showing the structure of the warp at a time $t = 313 \Omega(R = 1)^{-1}$, after the warp has settled to a quasi-steady state. The first panel shows a projection in the $y-z$ plane of a slice through the disc, and presents a global view of the warp. A closer view of the central regions is shown in the second panel, and illustrates how the warp and transition zone are confined to the central regions of the disc.

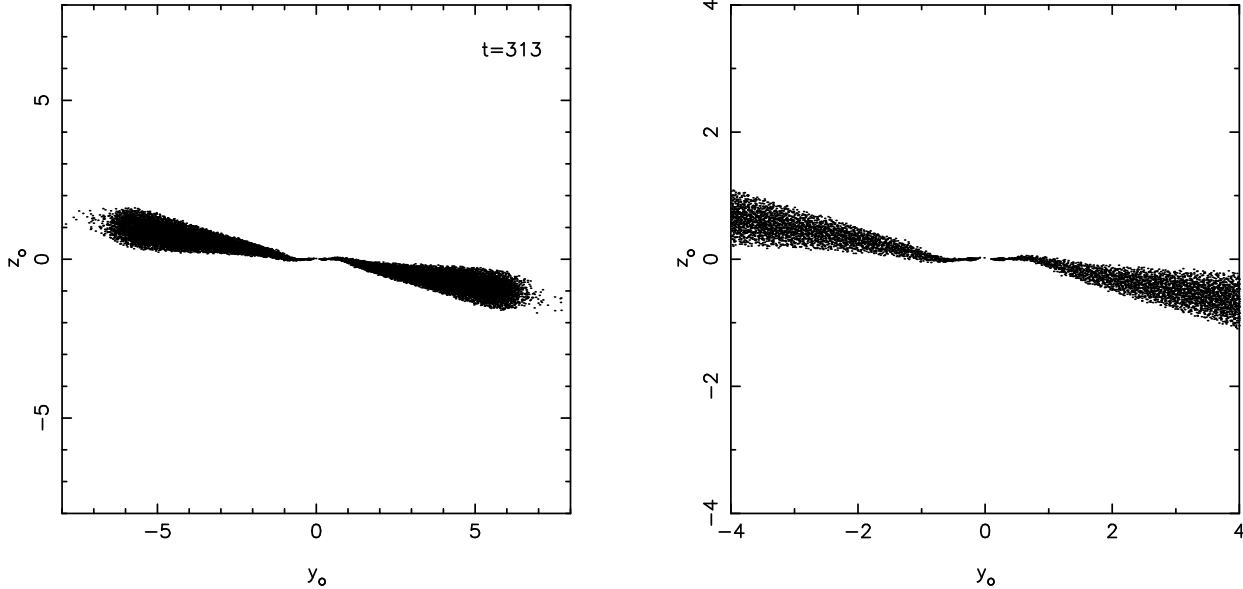


Figure 14. This figure shows the structure of the warp for run E6. A particle projection in the y - z plane of a slice through the disc is shown in the first panel illustrating the global structure of the disc. A close-up view of the warped region is shown in the second panel. The plots correspond to a time of $t = 313 \Omega(R = 1)^{-1}$. The differential precession time at the outer edge of the transition zone ($r = 2$) is $\tau_p = 166 \Omega(R = 1)^{-1}$.

8.5 Alignment Time Scale for Black Hole and Accretion Disc

As the calculations in the previous sections have shown, the effect of the Lense–Thirring precession induced by the dragging of inertial frames by a Kerr black hole is to cause the inner regions of a misaligned accretion disc to become aligned with the black hole angular momentum vector. Newton’s third law, however, implies that equal but opposite torques are exerted on the black hole by the disc, causing its angular momentum vector, in turn, to become aligned with the angular momentum vector of the outer disc material.

This process was considered by Rees (1978), who estimated the alignment time scale for the black hole and accretion disc by considering the mass flux through the disc. The direction of the angular momentum of this infalling matter is changed as it passes through the transition region between the aligned and misaligned disc, so that a simple estimate of the alignment time scale may be obtained from

$$\tau_{align} \simeq \frac{J_{BH}}{\dot{M} j_d(R_{BP}) \sin(i)}, \quad (32)$$

where J_{BH} is the black hole angular momentum, \dot{M} is the mass accretion rate through the disc, $j_d(R_{BP})$ is the specific angular momentum of disc material as it enters the warped region at R_{BP} , and i is the inclination angle between the outer disc and black hole equator. Using this general picture, Rees (1978) calculated the time scale for alignment in AGN and estimated it to be in the region of $\sim 10^8$ yr, comparable

to the ages of jets in AGN whose directions seem to have been constant over these time scales.

The above process was considered in more detail by Scheuer & Feiler (1996). These authors derived an analytic expression to describe the steady state warped structure of a disc around a Kerr black hole, using a linearized set of equations derived from those of Pringle (1992), to describe the evolution of a warped disc. By calculating the Lense–Thirring torque due to the black hole on this disc, they were able to calculate the reverse torque experienced by the black hole, and hence to estimate its alignment time scale. They found that the more detailed calculations gave time scales in essential agreement with the ideas proposed by Rees (1978), provided that the viscous diffusion coefficients acting in and out of the disc plane, ν_1 and ν_2 , are equal.

These estimates of the alignment time scale were calculated by assuming that disc warp is communicated through a disc on the standard viscous time scale, so that the transition radius R_{BP} is then expected to be at a large distance from the black hole. The calculations presented in previous sections indicate that when the full disc hydrodynamics are considered, then the evolution of warped discs changes substantially, such that the transition radius moves closer to the black hole. This effect has recently been considered by Natarajan & Pringle (1998), who have estimated alignment time scales of $\sim 10^5$ yr for black holes in AGN using the formula suggested by Scheuer & Feiler (1996), but taking into account differences between the viscous diffusion coefficients

that act in the plane and perpendicular to the plane of the disc.

The accretion disc models that we calculate may be different from those expected to occur in AGN, since they are relatively thick ($H/r \sim 0.08 - 0.03$), whereas $H/r \sim 10^{-3}$ may be more appropriate to the outer discs of AGN. In addition, they are of small radial extent. This prevents us from making detailed calculations of the alignment time scale for black holes in AGN on the basis of our calculations. Nonetheless, we can examine the rate at which the global disc tilt changes in the simulations, and compare it with that expected from the tilt evolution caused by the advection of misaligned angular momentum through the warped region, and with the work of Scheuer & Feiler (1996).

If the disc tilt in our simulations changes solely because of advection of material with misaligned J through the warped region, where it is torqued into alignment, then the rate of change of misaligned disc angular momentum may be estimated to be

$$\frac{dJ}{dt} \simeq \dot{M} j(R_{TS}) \sin(i), \quad (33)$$

where $j(R_{TS})$ is the specific angular momentum of disc material as it enters the warped region located at R_{TS} . The corresponding expression that applies when the transition zone occurs at the Bardeen–Petterson radius, R_{BP} is given by

$$\frac{dJ}{dt} \simeq \dot{M} j(R_{BP}) \sin(i), \quad (34)$$

where $j(R_{BP})$ is the specific angular momentum of disc material as it enters the region located at R_{BP} . By calculating \dot{M} from our simulations, we can estimate the effect of these processes, and the associated time scales for them to align the disc with the black hole and thus by Newton's third law, the time to align the black hole with the disc. We denote these time scales by τ_{TS} and τ_{BP} , respectively.

In our finite disc models, we expect the global change in the disc tilt to arise because of advection of tilt angular momentum through R_{TS} , viscous coupling between misaligned disc annuli, and residual torquing by the black hole on disc elements that lie somewhat beyond R_{TS} , which remains relatively close to the black hole in our simulations.

The time scale for the alignment of a black hole's spin angular momentum vector with that of the outer part of an accretion disc is given by Scheuer & Feiler (1996) to be

$$\tau_{align} \simeq \frac{1}{\pi \Sigma} \left(\frac{acM}{\nu_2 G} \right)^{1/2} \quad (35)$$

where a is the Kerr parameter, c is the speed of light, M is the black hole mass, Σ is the disc surface density, and ν_2 is the viscous diffusion coefficient acting on the disc warp. We remark that the expression of Scheuer & Feiler (1996) which gives the aligning torque (their equation [9]) indicates that most of the torque contribution arises from the region of the disc that is in the vicinity of the warp or transition radius, as was commented upon by these authors themselves, implying that the alignment time scale obtained is not reliant upon the disc being infinite, but just significantly larger than the transition radius.

This is also the case if the expressions for the tilt (24) and (25), applicable when α_1 is small, are used in order to

evaluate their expression for the torque. Then ν_2 in (35) should be replaced such that

$$\nu_2 \rightarrow \nu_2 \alpha_1 \frac{\left(\sqrt{(\epsilon^2 + \alpha_1^2)} + \epsilon \right)}{(\epsilon^2 + \alpha_1^2)}. \quad (36)$$

In addition for these cases $\nu_2 = c_B^2/(\alpha_1 \Omega)$. Note that in the Einstein precession case (25), the limit $\alpha_1 \rightarrow 0$, with both ν_2 and $\epsilon \propto 1/r$, is to be taken with the result that ν_2 is replaced by a constant value.

An interesting feature of the above is that in the case of prograde Einstein precession ($\epsilon > 0$) an alignment torque survives in the limit $\alpha_1 \rightarrow 0$, whereas in the retrograde case ($\epsilon < 0$), as occurs with softening, it vanishes. This is because of the short wavelength oscillations or bending waves in the former case. In the latter case the solution is evanescent and of the wrong phase, having zero twist, to produce an alignment torque. The above suggests that cases with prograde precession should show significantly larger twists and alignment torques than those with retrograde precession when the viscosity is small. This is found to be the case in our simulations.

The black hole alignment time scale may be written as

$$\tau_{align} \simeq \left| \frac{dJ}{dt} \right|^{-1} \left(\frac{GM^2 a \sin(i)}{c} \right) \quad (37)$$

By Newton's third law, the alignment torque acting on the black hole is equal and opposite to that acting to align the disc plane with the equatorial plane of the black hole. Thus, the alignment torque acting on the disc may be written

$$\frac{dJ}{dt} \simeq \pi \Sigma \left(\frac{\nu_2 G}{acM} \right)^{1/2} \left(\frac{GM^2 a \sin(i)}{c} \right). \quad (38)$$

We note that $S = G^2 M^2 a / c^3$, so that we may write equation (38) as

$$\frac{dJ}{dt} = \pi \Sigma (S \nu_2 GM)^{1/2} \sin(i). \quad (39)$$

In their discussion, Scheuer & Feiler (1996) distinguish between the viscosity coefficient, ν_1 , acting in the plane of the disc which is responsible for mass flow through the disc, and that which is responsible for the damping or diffusion of disc warp, ν_2 .

In the situation where the diffusion coefficients are equal (*i.e.* $\nu_2 = \nu_1$ where $\nu_1 = \alpha H^2 \Omega$) equation (39) may be written as

$$\frac{dJ}{dt} \simeq \pi \Sigma (S \nu_1 GM)^{1/2} \sin(i). \quad (40)$$

Recent work on the evolution of warped discs, including that presented in paper I, indicates that disc warp diffuses on a time scale much faster than that on which mass diffuses through the disc, and that the appropriate value for ν_2 is $\nu_2 = \nu_1 / (2\alpha^2)$. In order to estimate the alignment time scale for the black hole angular momentum vector, Natarajan & Pringle (1998) used this relation in equation (35). For our purposes of calculating the torque acting on the disc, using this relation in equation (39) leads to the expression

$$\frac{dJ}{dt} \simeq \frac{\pi \Sigma}{\alpha} \left(\frac{S \nu_1 GM}{2} \right)^{1/2} \sin(i). \quad (41)$$

We are able to compare our simulated disc alignment torques with the values expected from equations (33),

Run	R	\mathcal{M}	τ_m	τ_{TS}	τ_{BP}	τ_{SF2}	τ_{SF1}
S2	2	12	1363	11225	1348	119	3826
S6	2	30	1628	9573	1546	695	4096
E1	2	12	378	11225	1348	119	3826
E2	2	30	1120	10045	1570	869	4392
E6	7	14	4000	131367	18666	3219	56848

Table 2. The first column provides the label given to each run, the second column gives the radius. The third column gives the midplane mach number, and the fourth, fifth, sixth, seventh, and eighth columns give the measured and various analytically predicted alignment time scales, whose symbols are defined in the text. Note that calculation labels S_i indicate that the gravitational potential of the central object was softened, the labels E_i indicate that no softening was employed but that Einstein precession was included.

(34), (40), and (41). We denote the expected time scales for the discs to align with the black hole equatorial plane calculated from these equations as τ_{TS} , τ_{BP} , τ_{SF1} , and τ_{SF2} , respectively.

We denote the time scale for disc alignment measured from the simulations by τ_m . We define the time scales for disc alignment to be

$$\tau = |\mathbf{J}_\perp| \left(\frac{dJ}{dt} \right)^{-1} \quad (42)$$

where we take \mathbf{J}_\perp to be the perpendicular component of the angular momentum of the disc models at time $t = 0$. This value is used in the estimates of τ_m , τ_{TS} , τ_{BP} , τ_{SF1} , and τ_{SF2} .

The value of τ_m , the time scale for disc alignment measured from the simulations, was obtained by measuring the change in \mathbf{J}_\perp over time, and extrapolating forward to the point when $\mathbf{J}_\perp = 0$.

The values of \dot{M} used in equations (33) and (34), to estimate the values of τ_{TS} and τ_{BP} , were obtained from the simulations by measuring the mass flux through the disc models. The values of R_{TS} were taken from table 1 and the values of R_{BP} were calculated using equation (27). The values of ν_1 and α used in equations (40) and (41) were obtained from the measurements of \dot{M} and assuming a steady state such that $\dot{M} = 3\pi\nu\Sigma$. The values of α used in the calculation of the alignment time scales for each model were (S2 - $\alpha = 0.022$; S6 - $\alpha = 0.12$; E1 - $\alpha = 0.022$; E2 - $\alpha = 0.14$; E6 - $\alpha = 0.04$). These are very similar to the values of α_1 obtained from the bending wave calculations presented in paper I, and indicate that SPH produces a reasonably isotropic viscosity when applied to this problem.

The alignment time scales calculated from the simulations and the analytical torque estimates are presented in table 2. First of all, we consider the runs that employed softening of the gravitational potential, since in this case it is relevant to compare these calculations with the analytical estimates of the alignment time scales, given that the softening plays only a minor role in the simulations. The physical

models that lead to the analytical estimates of the alignment time scales do not include the effects of Einstein precession, and so strictly speaking they should not be compared with the results of calculations E1, E2, and E6 in which Einstein precession is included and plays an important role.

From table 2 we see that the results for the runs S2 and S6 indicate that the predicted alignment time scale, τ_{TS} , estimated by assuming that material is only torqued into alignment when it accretes through the transition zone, R_{TS} , is too long, indicating that the viscous torques acting between the aligned and misaligned disc components, and the residual torque due to the black hole beyond R_{TS} , are having a substantial effect on the evolution of the disc tilt. The alignment time scale τ_{SF2} leads to a prediction that the discs will align with the black hole equatorial plane on too short a time scale, whereas the estimate τ_{SF1} predicts too long a time scale. Interestingly, it appears that the estimate τ_{BP} based on equation (34) provides the best estimate of the alignment time scale in the cases S2 and S6.

The physical picture suggested by Rees (1978) is of a warped disc with constant mass flow in which the misaligned component of the disc material's angular momentum is transferred to the black hole as it passes through the warped region located at R_{BP} .

It may seem surprising that we obtain results for the alignment time scale that are consistent with Rees (1978) in view of the facts that the transition radius is much smaller in our case and (41) predicts a significantly faster rate. But we note that (41) is based on a linearized approximation which does not allow for the torques applied in the warped region of the disc to feedback into the disc structure. One would expect that this feedback would clear material with misaligned angular momentum from this region which would then have to be resupplied by mass accretion. This would result in a dependence of the alignment rate on the mass accretion rate.

From the discussion presented in section 4, we would expect that the alignment time scales obtained when Einstein precession is included would be noticeably shorter than when it is neglected. This arises because of the larger twist in these cases, leading to a larger torque. By examining the values of τ_m listed in table 2 we see that this is indeed the case. Comparing the runs S2 and E1, we see that the alignment time scale is shorter by a factor of ~ 4 when Einstein precession is included. Comparing runs S6 and E2, we observe the same trend, but at a reduced level because the transition zone is further from the black hole in these cases and the effects of Einstein precession are reduced accordingly.

By comparing the results of runs E1 and E6, we notice that τ_m is larger than in the latter case because of the larger disc size. Although the disc model parameters for these two cases differ slightly, giving slightly different transition radii, we would expect that the ratio of alignment time scales would be similar to the ratio of the initial disc angular momenta if the aligning torques are similar. We find that $\tau_m(E1)/\tau_m(E6) \sim 0.1$ and $J_\perp(E1)/J_\perp(E6) \sim 0.12$, suggesting that we not only calculate the position of the transition zone correctly with our smaller disc models with outer radii $r = 2$, but that we also accurately calculate the alignment torque between the outer and inner discs since this arises from the transition zone.

9 DISCUSSION AND CONCLUSION

In this paper we have performed simulations of accretion discs in orbit around a rotating black hole, which had its spin vector initially misaligned with that of the disc, in the lowest order post Newtonian approximation. Discs with midplane Mach numbers between 5 and 30 were considered. For discs with Mach numbers of 5, 9, and 12, the effective viscosity acting through the r - z component of the viscous stress, α_1 , is such that the warps are controlled by bending waves (see paper I). For the higher Mach number of 30, the warps evolve diffusively, but with an associated diffusion coefficient that is a factor of $\sim 1/(2\alpha_1^2)$ larger than that associated with mass flow through the disc (Papaloizou & Pringle 1983).

As expected the central portions of the disc models became aligned with the equatorial plane of the black hole out to a transition radius, beyond which the discs remained close to their original plane. This structure was established on the sound crossing, or warp diffusion, time. This period of initial relaxation to a well defined warped disc structure was followed by a period of evolution occurring on a longer time scale, corresponding to solid body precession of the disc and a slow process of alignment of the outer disc with equatorial plane of the black hole. Both of these are caused by the fact that we are forced to consider isolated discs of finite radii for reasons of numerical tractability. Nonetheless the position of the transition between the aligned and misaligned disc components is not affected by this. Because of the much more effective communication of warps than implied by the standard viscous time scale, the transition radius was found to be much smaller than that given by Bardeen & Petterson (1975), ranging between 15 and 30 gravitational radii for a hole with Kerr parameter $a = 1$.

In the warped regions of the disc with changing inclination, the expected vertical shear (Papaloizou & Pringle 1983) was seen in the simulations. We found that these velocities were limited to be subsonic, presumably by nonlinear effects such as shocks. An interesting issue is the stability of this shear flow. Parametric instability associated with bending waves is a possibility (Papaloizou & Terquem 1995; Gammie, Goodman, & Ogilvie 1998, private communication). This may produce a level of turbulence in a disc with low viscosity. But it should be noted that the SPH simulations presented here are for discs that are already viscous, such that the growth rate of any instability is exceeded by the viscous damping. Simulations with a viscosity small enough to investigate shear flow instability require too many particles to be practicable at present.

Models were considered both at high and low inclination. In the nonlinear high inclination case, although the transition radius remained approximately in the same location, the transition was more abrupt than in the low inclination case, indicative of a tendency for the outer part of the disc to become disconnected from the inner part. The implications of this are that a disc which is forced to maintain a nonlinear warp due to severe misalignment will tend to break into two or more disconnected pieces, rather than maintain a smoothly warped structure in which the perturbed horizontal motions remain transonic.

Although the calculations performed here are in a very different physical regime to that expected for discs around AGN, the time scale we obtain for black hole – disc align-

ment is in essential agreement with the ideas of Rees (1978) and accordingly the later work of Scheuer & Feiler (1996), if the viscous diffusion coefficients acting in and out of the disc plane are taken to be equal. We also found that this alignment time scale could be significantly shortened by the inclusion of Einstein precession, in line with the predictions of a linear analysis.

REFERENCES

- Blandford, R.D., 1996, *Gravitational Dynamics*, C.U.P, eds. R. & E. Terlevich.
- Bardeen, J.M., Petterson, J.A., 1975, *ApJ(Letters)*, 195, L65.
- Gingold R.A., Monaghan J.J., 1977, *MNRAS*, 181,375
- Hatchett, S.P, Begelman, M.C., Sarazin, C.L., 1981, *MNRAS*, 247, 677
- Ivanov, P.B., Illarianov, A.F., 1997, *MNRAS*, 285, 394
- Kumar, S., Pringle, J.E., 1985, *MNRAS*, 213, 435
- Lucy L.B., 1977, *AJ*, , 83, 1013
- Natarajan, P., Pringle, J.E., 1998, *ApJ*, 506, L97
- Nelson R.P., Papaloizou J.C.B., 1994, *MNRAS*, 270, 1
- Nelson R.P., Papaloizou J.C.B., 1999, *MNRAS*, submitted (Paper I).
- Nelson, R.P., Papaloizou, J.C.B., Terquem, C., 1999, *Astrophysical Discs – An EC Summer School*, P. 81, *Astronomical Society of the Pacific*, Eds. J.A. Sellwood & J. Goodman
- Papaloizou, J.C.B., Terquem, C., 1995, *MNRAS*, 274, 987
- Papaloizou, J.C.B., Pringle, J.E., 1983, *MNRAS*, 202, 1181
- Papaloizou, J.C.B., Lin, D.N.C., 1994, *Theory of Accretion Discs– 2*, 329–340, *Kluwer Academic Publishers*, Eds W.J. Duschl.
- Papaloizou, J.C.B., Lin, D.N.C., 1995, *ApJ*, 438, 841
- Pringle, J.E., 1992, *MNRAS*, 258, 811
- Rees, M.J., 1978, *Nat*, 275, 516
- Scheuer, P.A.G., Feiler, R., 1996, *MNRAS*, 282, 291
- Shakura N.I., Sunyaev R.A., 1973, *A&A*, 24, 337